

How concerted are ionic hops in inorganic solid-state electrolytes?

Cibrán López,^{1,2,3} Riccardo Rurali,³ and Claudio Cazorla^{1,2}

¹*Departament de Física, Universitat Politècnica de Catalunya, 08034 Barcelona, Spain*

²*Barcelona Research Center in Multiscale Science and Engineering,
Universitat Politècnica de Catalunya, 08019 Barcelona, Spain*

³*Institut de Ciència de Materials de Barcelona, ICMA-B-CSIC, Campus UAB, 08193 Bellaterra, Spain*

Despite being fundamental to the understanding of solid-state electrolytes (SSE), little is known on the degree of coordination between mobile ions in diffusive events. Thus far, identification of concerted ionic hops mostly has relied on the analysis of spatio-temporal pair correlation functions obtained from atomistic molecular dynamics (MD) simulations. However, this type of analysis neither allows for quantifying particle correlations beyond two body nor determining concerted ionic hop mechanisms, thus hindering a detailed comprehension and possible rational design of SSE. Here, we introduce an unsupervised k-means clustering approach able to identify ion-hopping events and correlations between many mobile ions, and apply it to a comprehensive *ab initio* MD database comprising several families of inorganic SSE and millions of ionic configurations. It is found that despite two-body interactions between mobile ions are largest, higher-order n -ion ($2 < n$) correlations are most frequent. Specifically, we prove an universal exponential decaying law for the probability density function governing the number of concerted mobile ions. For the particular case of Li-based SSE, it is shown that the average number of correlated mobile ions amounts to 10 ± 5 and that this result is practically independent of temperature. Interestingly, our data-driven analysis reveals that fast-ion diffusion strongly and positively correlates with ample hopping lengths and long hopping spans but not with high hopping frequencies and short interstitial residence times. Finally, it is shown that neglectation of many-ion correlations generally leads to a modest overestimation of the hopping frequency that roughly is proportional to the average number of correlated mobile ions.

INTRODUCTION

Solid-state electrolytes (SSE) presenting high ionic conductivity are pivotal for the development of transformative green-energy conversion and storage technologies like fuel cells, electrocatalysts and solid-state batteries [1–4]. SSE are complex materials that exhibit very disparate compositions, structures, thermal behaviors and ionic mobilities hence, unfortunately, it is difficult to rationally ascribe them to general categories and design principles [5, 6]. In particular, there is a lack of fundamental knowledge on the collective atomistic mechanisms that govern ionic transport.

In recent years, analysis of the correlations between ionic transport (i.e., mobile ions) and lattice dynamics (i.e., vibrating ions) have attracted increasing interest [6–9]. The “paddle-wheel” mechanism, in which the libration of semirigid anionic units can propel cation transport [10], is a well-known example of such a possible type of atomic concertation in superionic materials. The influence of lattice anharmonicity on ionic transport has been also thoroughly discussed, both theoretically and experimentally [11–14]. Nonetheless, very little is known on the existing level of coordination between many mobile ions in diffusive events.

Thus far, identification of correlations between mobile ions mostly has relied on the analysis of van Hove correlation functions obtained from *ab initio* molecular dynamics (AIMD) simulations and on zero-temperature nudged elastic band (NEB) calculations [15–17]. For Li-based SSE, it has been theoretically demonstrated that concertation between many mobile ions tends to lower the en-

ergy barriers for ionic diffusion, hence collective diffusive behaviour, rather than individual ionic hops, is expected to be predominant in superionic materials [17].

Nevertheless, due to the inherent limitations of the analysis methods employed up to now, many questions on the exact level of concertation between many mobile ions remain unanswered. For example, how many ions are typically coordinated in diffusive events and through which collective mechanisms? Are these many-ions correlations dependent on temperature or not? Can collective hopping behaviour be analytically described by a general law? Does the degree of ionic coordination depend on the specific family of SSE or is universal? How the neglectation of many-ion correlation affects the estimation of key atomistic quantities like the ion hopping frequency? Answering these questions is not only relevant from a fundamental point of view, it is also necessary to justify the broad adoption of formulas obtained in the dilute-solution limit (e.g., the Nerst-Einstein relation for the ionic conductivity) which assume mobile ions to be fully uncorrelated [18–22].

In this work, we introduce a k-means clustering approach able to unsupervisedly identify ion-hopping events and quantify correlations between many mobile ions from ionic configurations generated in atomistic molecular dynamics simulations. This automatized analysis was recursively applied on a comprehensive AIMD database comprising several families of inorganic SSE and millions of atomic configurations [6, 25]. It was found that many-ion correlations beyond pairwise are dominant in diffusive events and can be represented by an universal exponential decaying law. Interestingly, for Li-based SSE it was

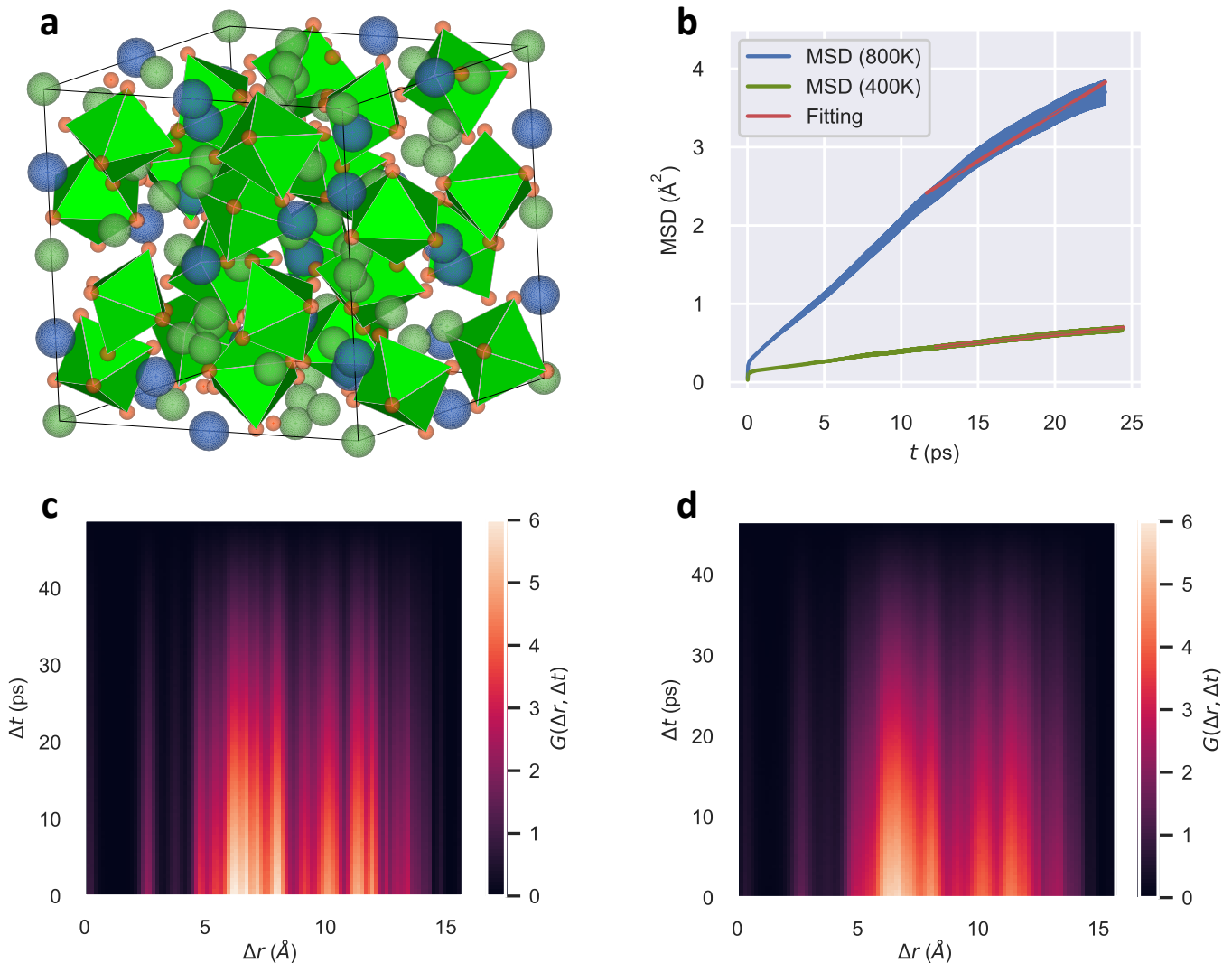


FIG. 1. **Standard characterization of ionic transport and correlations in SSE from molecular dynamics simulations particularized for $\text{Li}_7\text{La}_3\text{Zr}_2\text{O}_{12}$ (LLZO).** (a) Ball-stick representation of bulk LLZO with a tetragonal crystal structure and space group $I4_1/acd$; lanthanum, lithium, oxygen and zirconium atoms are represented with blue, green, red and blue spheres, respectively. (b) Mean squared displacement of Li cations obtained from DFT-AIMD simulations performed at $T = 400$ and 800 K. (c)–(d) Van Hove correlation function for Li cations (in arbitrary units) obtained from DFT-AIMD simulations performed at $T = 400$ and 800 K, respectively.

determined that the average number of concerted mobile ions amounts to 10 ± 5 , very much independently of temperature. Moreover, the introduced unsupervised analysis also permitted us to accurately quantify the prevalent correlations between ionic diffusion and key microscopic quantities like ion hopping lengths and frequencies and interstitial residence times. In addition, the effects of neglecting many-ion correlations on the estimation of the ion hopping frequency and migration energy barrier were substantiated. Therefore, the present work leverages our fundamental understanding of technologically relevant SSE and elaborates on the adequacy of employing formulas obtained within the dilute-solution limit for describing them.

RESULTS

Figure 1 shows the results of finite-temperature AIMD simulations performed for $\text{Li}_7\text{La}_3\text{Zr}_2\text{O}_{12}$ (LLZO), an archetypal Li-based SSE [23]. LLZO is a complex oxide material with garnet-like structure (space group $I4_1/acd$, Fig. 1a) that presents high lithium-ion conductivity and excellent thermal and chemical stabilities. As it is customarily done for SSE, one can estimate the tracer Li diffusion coefficient of LLZO, D_{Li} , directly from the configurations generated during AIMD simulations by computing the time derivative of the corresponding mean squared displacement (Fig. 1b and Methods) [8, 24]. Larger D_{Li} values are associated with larger ionic conduc-

tivities, σ_{Li} , as deduced from the popular Nernst-Einstein relation obtained in the dilute-solution limit:

$$\sigma_{\text{Li}} = \frac{z_{\text{Li}}F}{k_B T} \cdot D_{\text{Li}}, \quad (1)$$

where z_{Li} represents the charge of the mobile ion, k_B the Boltzmann constant and $F = e \cdot N_A$ the Faraday constant (e is the electron charge and N_A the Avogadro's number).

The van Hove correlation function, $G(\Delta r, \Delta t)$ (Methods), provides information on the spatio-temporal distribution of pairs of particles in atomistic configurations obtained from finite-temperature MD simulations (e.g., for a null time span G is equivalent to the usual radial pair distribution function). Figures 1c,d show the van Hove correlation function of Li atoms estimated for superionic LLZO at two different temperatures; it is appreciated that pair correlations between nearby ions (i.e., $2 \leq \Delta r \leq 5 \text{ \AA}$) are substantial over time spans of several tens of picoseconds, since $G(\Delta r, \Delta t)$ remains discernible within those variable intervals. At the highest simulated temperature, ionic diffusion is sizeable (Fig. 1b) and the peaks of the van Hove correlation function (Fig. 1d) get noticeably faded (barely change) along the interparticle distance (time) dimension in comparison to those obtained for the non-superionic state (Fig. 1c). For completeness purposes, the ‘‘self’’ and ‘‘distinct’’ components of the lithium van Hove correlation function (Methods) are shown in Supplementary Fig.1. These $G(\Delta r, \Delta t)$ results clearly show the existence of significant ion-pair correlations in LLZO ionic diffusion.

Nevertheless, the standard particle correlations analysis presented above is too restricted since it only considers correlations between pairs of atoms, thus neglecting any possible higher-order level of n -ion ($2 < n$) concertation. In addition, it does not provide any atomistic insight into the many-ion mechanisms involved in ionic diffusion. To overcome this type of limitations, we devised an algorithm based on k-means clustering that is able to unsupervisedly identify ion-hopping events and correlations between many particles, and applied it to a comprehensive AIMD database of inorganic SSE [6, 25]. The introduced algorithm also permits to automatically identify ion hopping lengths and frequencies and interstitial residence times, hence the general dependencies between these atomistic descriptors and ionic diffusion can be determined.

K-means clustering algorithm for unsupervised identification of ionic hops and diffusive paths

Our approach consists in identifying the equilibrium and metastable positions in a supercell around which particles vibrate; subsequently, the temporal sequence of atomic displacements from one of those vibrational centers to another are monitored thus determining ion diffusion paths without imposing any restriction. Only two fundamental premises are assumed in our procedure,

namely, the vibration of ions around equilibrium and metastable positions are roughly isotropic, and diffusion events are less frequent than atomic vibrations.

K-means clustering is an unsupervised machine learning algorithm that classifies objects in such a way that elements within a same group, called ‘‘cluster’’, are in a broad sense more similar to each other than to elements in other clusters. Our method for identifying vibrational centres from sequential ionic configurations relies on k-means clustering (Methods) since this approach assumes isotropy on the fluctuations of non-diffusive particles. (It is worth mentioning that spectral clustering, based on interparticle connectivity instead of interparticle distance, was also considered, however less satisfactory ionic hops identification results were obtained in this case.) Importantly, the definition of arbitrary materials-dependent threshold distances for scrutiny of ionic hops is completely avoided in our approach, as we explain next.

For each individual ionic trajectory, the optimal number of clusters, K , which represents the number of vibrational centres that the particle visits during the simulation, is systematically selected as the one that maximises the silhouette coefficient averaged over all the samples corresponding to cases $2 \leq K$ (Methods). Silhouette coefficients, S , are individually ascribed to each cluster and can take values within the interval $[-1, +1]$. S values near $+1$ indicate that the sample is far away from the neighbouring clusters. On the other hand, negative S values indicate that the sample might have been assigned the wrong cluster (an exact zero value would indicate that the sample is on the decision boundary between two neighbouring clusters). Nevertheless, this procedure fails to describe the case of a non-diffusive particle, which would correspond to $K = 1$, since by construction $2 \leq K$. To avoid this issue, whenever the maximum average silhouette coefficient is below an arbitrary, but reasonable, threshold value of 0.7, we automatically impose $K = 1$ (i.e., the ion does not diffuse throughout the simulation). The dependence of our algorithm performance on such a threshold value has been exhaustively tested, finding negligible effects on the final outcomes.

Once the number of vibrational centres, their real-space location and temporal evolution are determined, ionic diffusive paths are defined like the sections connecting two different vibrational centres over time. In our calculations, it is appreciated that, due to the discrete nature of the generated ionic trajectories, diffusive paths generally start and finish at around 0.5 \AA from their defining vibrational centres. An illustrative example of our method for identification of vibrational centres and ionic diffusive paths is shown in Fig. 2a. Therein, two vibrational centres with a highly confident average silhouette coefficient value of 0.88 (green and yellow points) are depicted along with the ionic diffusive path (blue points) that connects them. Our algorithm was recursively applied to a comprehensive DFT-AIMD database involving different families of SSE [6, 25] (Supplementary Tables 1–3), obtaining in all the cases highly accurate results for

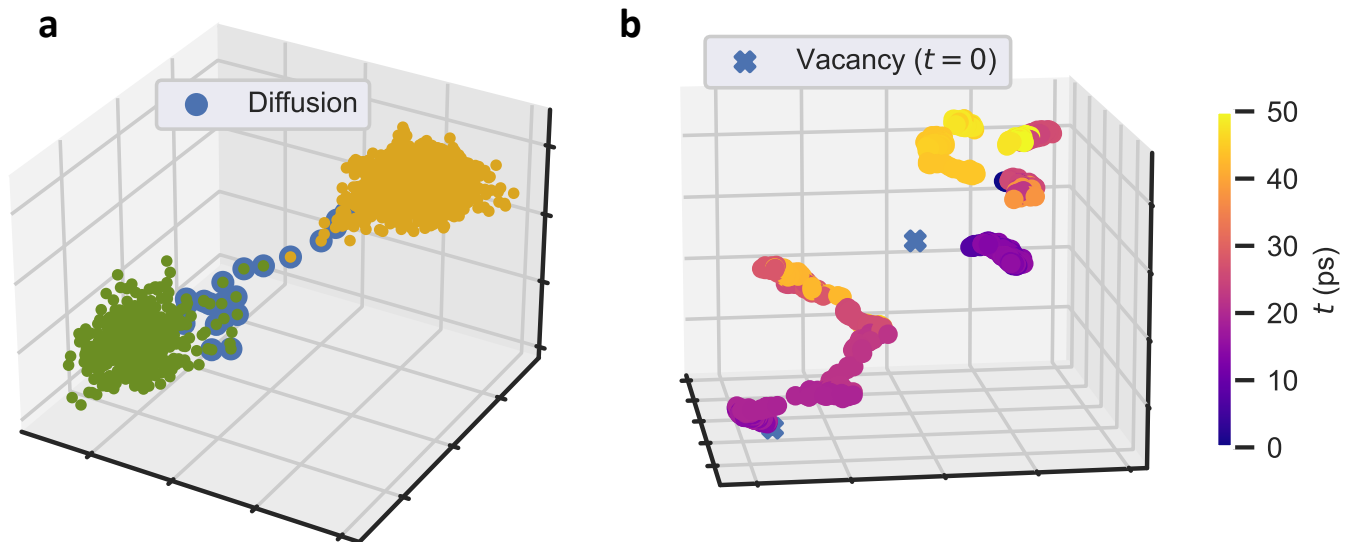


FIG. 2. **Unsupervised k-means clustering algorithm for identification of ionic hops and diffusion paths.** (a) Ionic diffusion of an arbitrary mobile atom in a DFT-AIMD simulation of LLZO performed at $T = 400$ K (blue circles). The two vibration centers defining the origin and end of the ionic hop are represented with orange and green points, respectively. (b) Temporal sequence of ionic hops identified for a ≈ 50 ps duration DFT-AIMD simulation of LLZO performed at $T = 400$ K. Blue crosses represent the initial position of two lithium vacancies introduced in the simulation cell; ionic hops are initiated near them. Different sections of a same diffusion path do not necessarily correspond to a same ion.

the identification of ionic hops and diffusive paths. For example, for non-stoichiometric LLZO (i.e., containing Li vacancies) simulated at temperatures of 400 and 800 K, reassuring average silhouette coefficients amounting to 0.99 and 0.97 were respectively obtained (Fig. 2b).

It is worth noting that our ionic hop identification algorithm neither presupposes a fixed number nor the positions of the vibrational centres in the provided atomistic configurations (e.g., the number of vibrational centres may differ from the number of potentially mobile atoms when there is significant ionic diffusion). This adaptability feature turns out to be particularly useful for the identification of metastable crystalline positions (e.g., interstitials) and evaluation of residence times, as we will show later on. The analysis method just explained has been implemented in the `IonDiff` software [26], a freely available open-source python code (Methods).

Quantitative analysis of concertation between many mobile ions

The ionic hop identification approach explained above was applied to a comprehensive DFT database of inorganic SSE comprising a total of 83 AIMD simulations (Methods) in which ionic diffusion was substantial [6, 25]. Since we are primarily interested in unveiling universal behaviours and relationships in ionic transport, we considered different Ag-, Cu-, halide-, O-, Na- and Li-based superionic compounds (Supplementary Tables 1–3). To quantitatively evaluate the correlations and level of concertation between an arbitrary number of mobile ions, n ,

we devised and implemented the following algorithm.

For a given sequence of ionic configurations generated during a molecular dynamics simulation, the corresponding correlation matrix for diffusive events was computed. To this end, we first assigned a value of “1” to each diffusing particle and of “0” to each vibrating particle at each simulated time frame (Fig. 3a). Such a binary numerical assignment was straightforwardly performed with the ionic hop identification algorithm introduced in the previous section. Due to the discrete nature of the generated ionic trajectories, and to improve numerical convergence in the subsequent correlation analysis, the obtained multi-step time functions were approximated with Gaussians that equaled the half maxima at their width (Fig. 3a, in analogy to the “full-width-at-half-maximum” –FWHM– method widely employed in signal processing). Subsequently, we computed the $N \times N$ correlation matrix, where N is the number of potentially mobile ions, resulting from all the gathered simulation data; this latter step involves the calculation of covariance coefficients for ions taken in pairs [6].

The correlation matrix thus estimated, however, may be difficult to converge due to its statistical character (particularly in situations for which the number of mobile ions and time steps are somewhat limited, as it tends to be the case of computationally intensive AIMD simulations). To overcome these practical issues, we numerically computed a reference correlation matrix corresponding to a randomly-distributed sequence of ionic hops with Gaussian FWHM equal to the mean diffusion time determined for the scrutinised simulation (note that due to the finite width of the Gaussians such a correla-

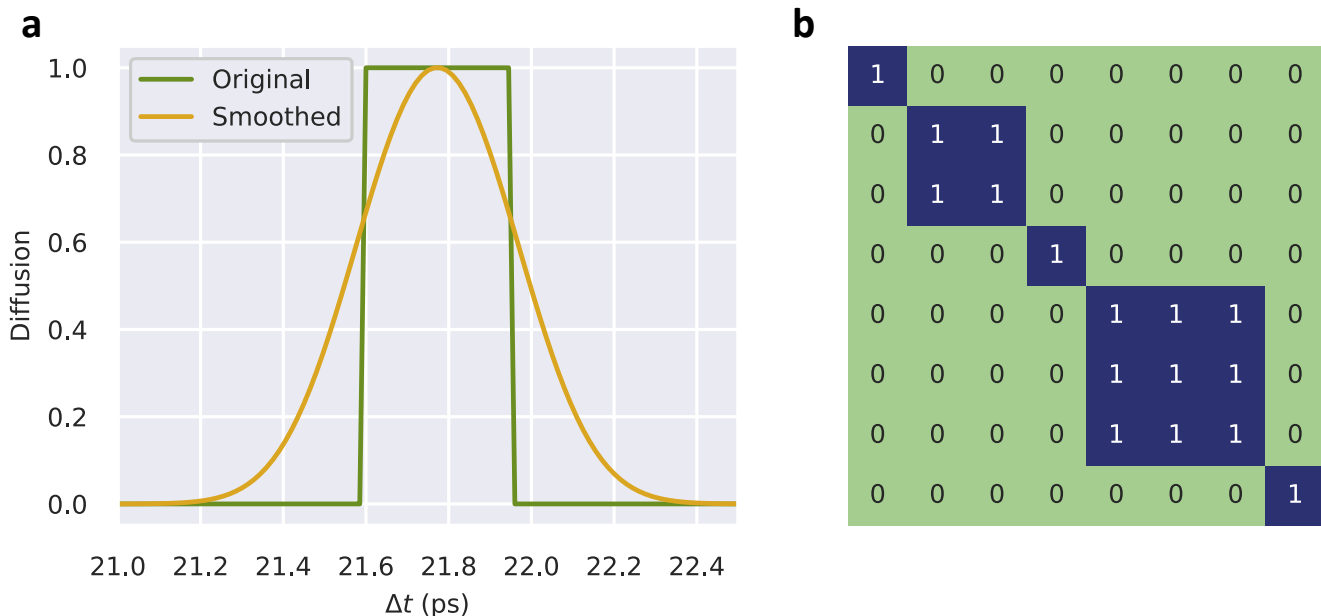


FIG. 3. **Unsupervised estimation of correlations between many mobile ions.** (a) At each time step, the state of each mobile ion is identified with a “0”, if it is vibrating, or a “1”, if it is hopping. The multi-step functions obtained over time are smoothed out with Gaussian functions to improve the numerical convergence in the subsequent calculation of the many-ion correlation matrix. (b) Considering all the binary data generated during a molecular dynamics simulation, a $N \times N$ correlation matrix is obtained, N being the number of possible mobile ions, which provides the number and indexes of uncorrelated and correlated ions (represented by “0” and “1”, respectively). In the provided example, a group of two ions and another of three move concertedly, while three particles remain uncorrelated during the whole simulation.

tion matrix is not exactly equal to the identity). Subsequently, covariance coefficients in the original correlation matrix larger (smaller) than the corresponding random reference values were considered as true correlations (random noise), hence were rounded off to one (zero) for simplification purposes. In order to not underrate the many-ion correlations, different hops of a same ion were treated as independent events.

In this manner, a correlation matrix consisting of ones and zeros is finally assembled from which one can easily determine how many and which particles remain concerted during diffusion. Figure 3b, shows a correlation matrix example in which a group of two mobile atoms and another of three move concertedly, while three ions remain uncorrelated during the whole simulation (rows and columns have been reshuffled in order to facilitate the visualisation of many-ion correlations). The described many-ion correlation identification algorithm also has been implemented in the IonDiff software [26], a freely available open-source python code (Methods).

Probability density function governing the number of correlated mobile ions

Figure 4a shows the probability density function (pdf) that governs the number of concerted ions in diffusive events estimated for different SSE families (i.e., averaged

over compounds belonging to a same category and temperature). These results were obtained from AIMD simulations that fully take into account anharmonicity and temperature effects.

In all the cases, an exponential decaying function was found to fairly reproduce the estimated distribution of n -concerted ions (solid lines in Fig. 4a). Consequently, the degree of concertation between mobile particles is always largest for pairs of ions and steadily decreases for increasing number of ions (here, we arbitrarily but reasonably considered only cases up to $n = 20$). The value of the pre-exponential factor and parameter in the exponential function, however, significantly vary from one family of materials to another. Therefore, the level of many-ion coordination in diffusive events depends on the specific SSE group. In particular, O-, halide- and Na-based fast-ion conductors exhibit the most rapidly decaying pdf profiles, meaning that correlations for a large number of mobile ions are smallest. On the other hand, Cu- and Li-based fast-ion conductors display the most slowly decaying pdf profiles (i.e., correlations for a large number of mobile ions are largest), while Ag-based SSE render an intermediate trend.

Figure 4b shows the general probability density function obtained for the number of concerted mobile ions in fast-ion conductors (i.e., averaged over all SSE families and temperature). An exponential decaying law is found to reproduce remarkably well the estimated dis-

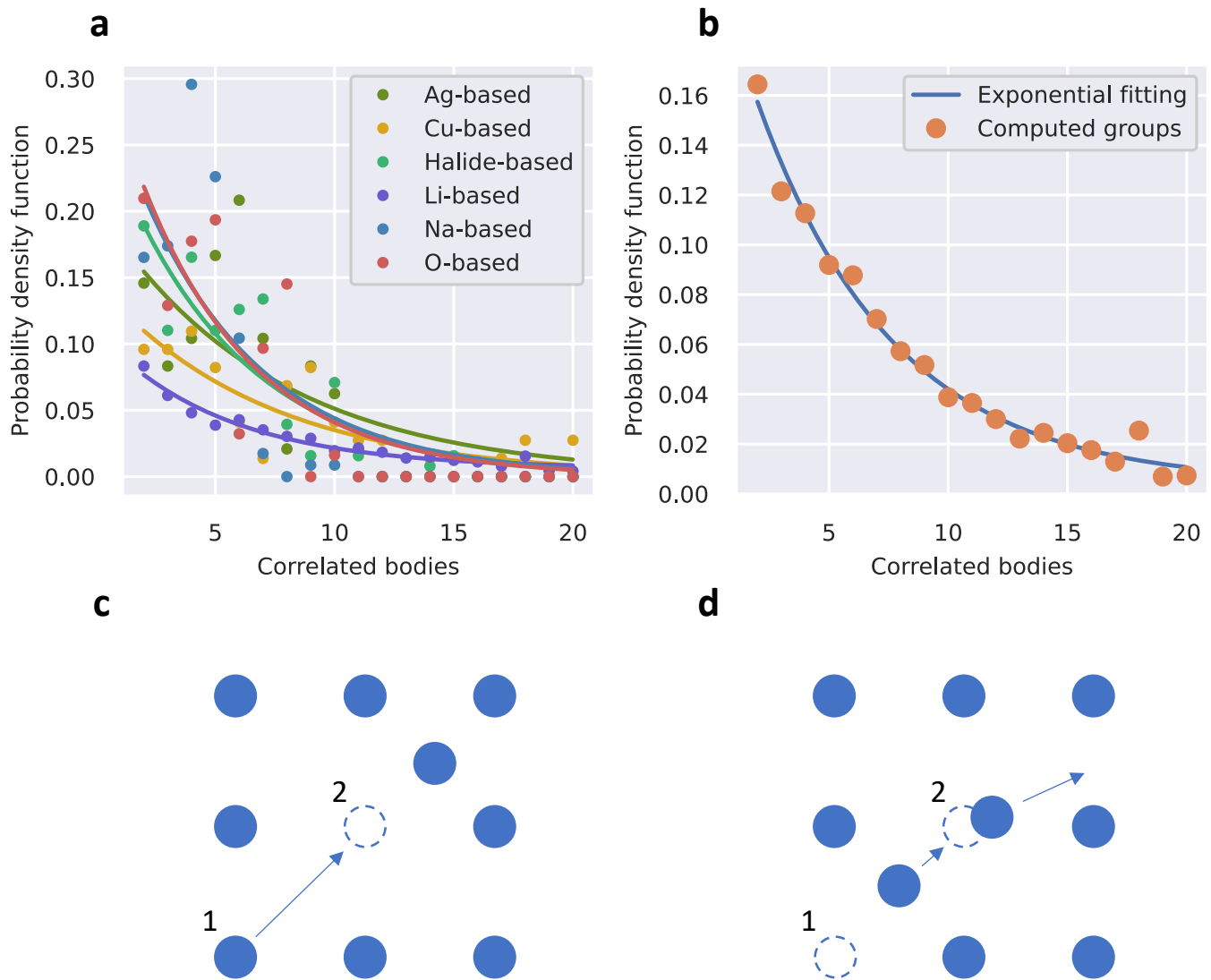


FIG. 4. Many-ion correlation results obtained from applying the introduced unsupervised k-means clustering algorithm on a comprehensive DFT-AIMD database of inorganic SSE [25]. (a) Probability distribution function for the number of coordinated ions in collective ionic hops estimated separately for each SSE family. High-order many-ion correlations are most substantial in Cu- and Li-based superionic materials. Solid lines represent exponential decaying fits to the data points. (b) General probability distribution function for the number of coordinated ions in collective ionic hops estimated considering all SSE compounds. An exponential decaying function of the form $f(n) = 0.220 \cdot \exp(-0.252n)$ fits fairly well the obtained data points. Two different two-ion coordinated mechanisms were most frequently observed in diffusive events: (c) ion (1) moves towards an empty equilibrium lattice position just left by ion (2), and (d) a mobile ion (1) kicks out a vibrating atom (2) and occupies its equilibrium lattice position.

tribution of n -ion correlations. In this general case, the degree of particles concertation is also largest for pairs of ions, as expected. However, by performing integrations of the area enclosed below the solid line in Fig. 4b, it is found that coordinated diffusive events involving more than two ions turn out to be more frequent (roughly by a factor of 6). This finding, which follows from comprehensive AIMD simulations and is not restricted to a unique SSE family, is consistent with previous computational results reported for Li-based materials [17].

Our formalism also allows to identify which particles participate in the disclosed n -ion coordinated diffusion events, which is very convenient for data visualization purposes. For the special case of $n = 2$ correlated diffusion processes, we determined the two most relevant atomistic coordination mechanisms, which are sketched in Figs. 4c,d. The first mechanism consists in a sequence of two diffusion events in which a first mobile ion hops to an interstitial position leaving a vacant site that is immediately occupied afterwards by a second diffusing particle

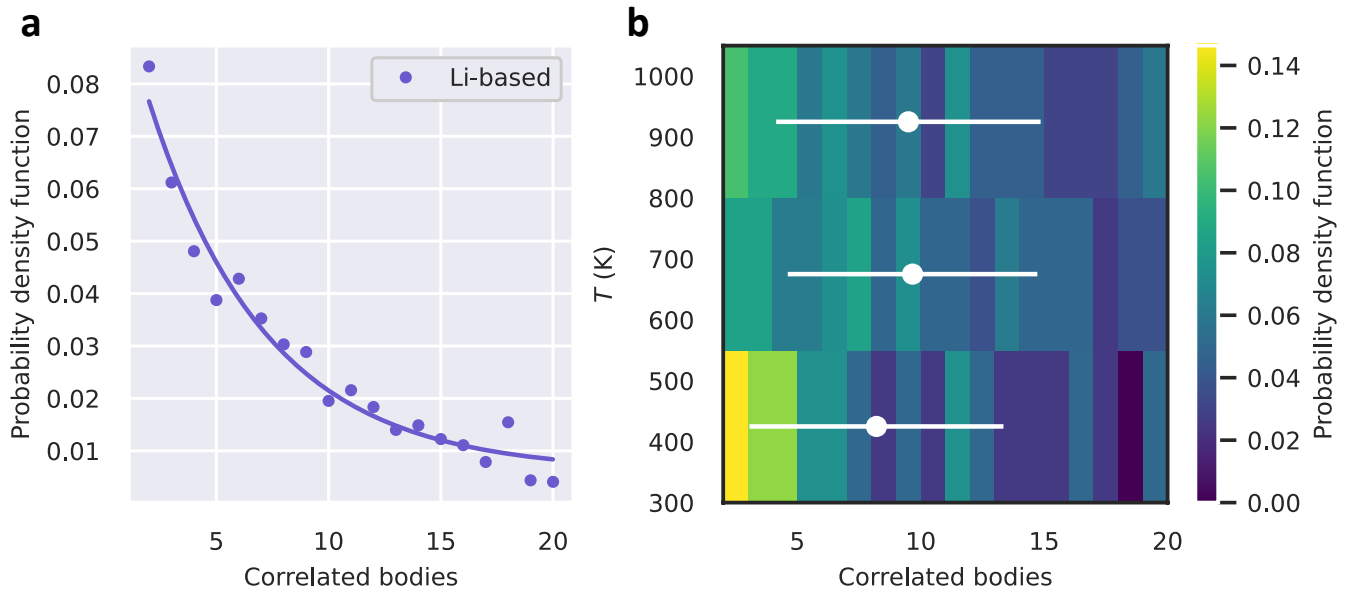


FIG. 5. **Many-ion correlation results obtained for Li-based SSE.** (a) Probability distribution function for the number of concerted ions in diffusive events. The solid line represents an exponential decaying fit to the data points. (b) Temperature-dependence of the probability distribution function shown in (a) considering the intervals $300 \leq T_1 \leq 550$ K, $550 \leq T_2 \leq 800$ K and $800 \leq T_3 \leq 1050$ K. White dots and lines denote average values and corresponding standard deviations, respectively.

(Fig. 4c). The second mechanism consists in the forced jump of a particle resulting from the direct influence of a second diffusing ion (Fig. 4d). It is worth noting that these two $n = 2$ ionic correlation mechanisms have been already reported in the literature for Li-based compounds [27], thus confirming the reliability of our unsupervised ionic-hop identification approach.

Temperature dependence of many mobile ions correlations

An interesting question to answer for superionic materials is whether the degree of concertation between many mobile ions depends on temperature or not [18, 19, 28]. The findings reported in the previous section cannot provide direct insights into this question since were obtained from thermal averages. Consequently, we performed a detailed temperature analysis of the many-ion correlations identified for Li-based compounds alone, since these are technologically very relevant and relatively abundant.

Figure 5a shows the pdf estimated for the number of concerted many mobile ions in Li-based SSE (same as in Fig. 4a). By taking all the collective diffusive events represented in that figure, we constructed normalised temperature histograms considering the three intervals $300 \leq T_1 \leq 550$ K, $550 \leq T_2 \leq 800$ K and $800 \leq T_3 \leq 1050$ K, as shown in Fig. 5b. Very mild differences are appreciated for the pdf's estimated for such temperature ranges. For example, at low temperatures coordinated diffusion events involving pairs of ions appear to be more frequent than at high temperatures.

However, when average quantities are considered, such moderate discrepancies mostly disappear. Specifically, the average number of coordinated mobile ions approximately amounts to 10 ± 5 for all the investigated temperature intervals (white dots and lines in Fig. 5b). Therefore, we may conclude that the level of concertation between mobile ions in Li-based SSE is practically independent of temperature.

Relationship between ionic diffusion and key atomistic descriptors

As explained in previous sections, the IonDiff software [26] allows to determine the centers of vibration and exact migrating paths of ions as provided by molecular dynamics simulations. Accordingly, for a given sequence of ionic configurations, it is straightforward to estimate insightful atomistic descriptors like the average hopping distance, Δr , hopping time, Δt , and hopping frequency, ν . Likewise, it is also possible to estimate interstitial residence times, γ , by monitoring the simulation time during which a particle remains fluctuating around a metastable position (e.g., interstice). The identification of metastable positions was performed by comparing the centers of vibration obtained during a whole simulation with those of the perfect equilibrium configuration, and assuming that metastable and equilibrium vibrational centers should be separated by a distance of at least 1.0 \AA (Supplementary Fig.2).

Figure 6 shows the level of correlation estimated for the tracer ion diffusion coefficient, D_x , and atomistic de-

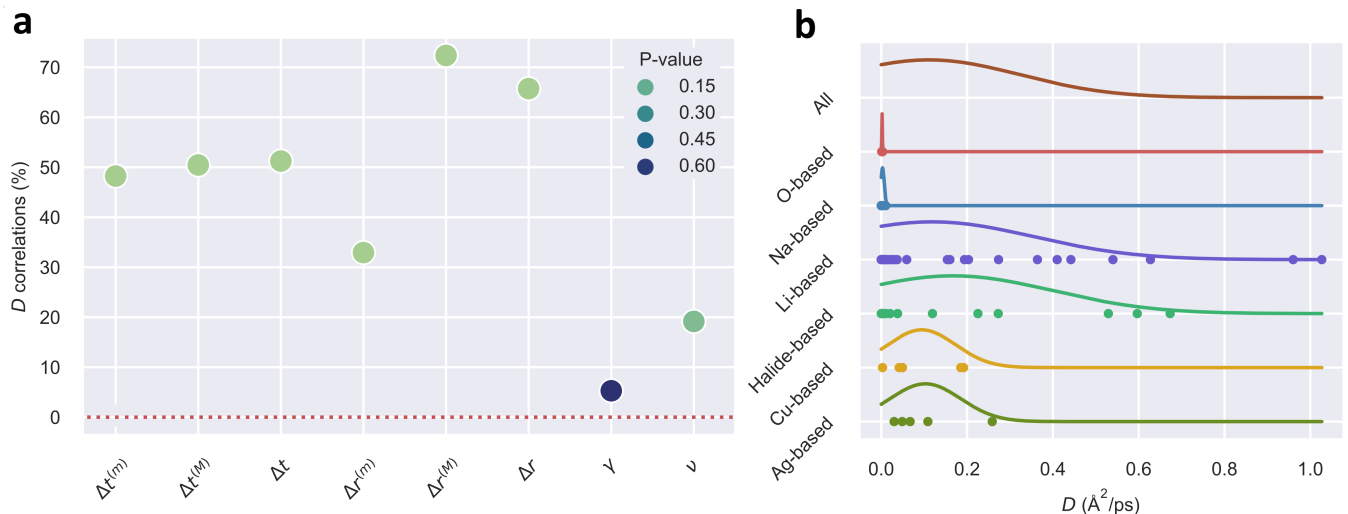


FIG. 6. **Correlations between ionic diffusion and key atomistic descriptors.** (a) D stands for the tracer ion diffusion coefficient, Δt the average duration of an ionic hop, Δr the average length of an ionic hop, γ the average interstitial residence time and ν the hopping frequency. Superscripts “(M)” and “(m)” denote maximum and minimum values estimated for the corresponding descriptor. (b) Distribution of tracer ion diffusion coefficients calculated for each SSE family.

criptors described above considering all the SSE families examined in this study (for this analysis, we considered the tracer diffusion coefficient instead of the full ion diffusion coefficient [19–21] because of its ubiquity in computational studies). Such correlations were obtained by following the same data-analysis approach that was introduced in work [6], which essentially involves the computation of Spearman correlation coefficients and p -values for the assessment of statistical significance. Besides examining average quantities, for the case of Δr and Δt we also considered their maximum, “(M)”, and minimum, “(m)”, values. Several interesting conclusions follow from the results shown in Fig. 6a.

The largest D_x correlations involving average quantities are found for the hopping length and hopping time, which are both positive and roughly amount to 65 and 50%, respectively. In the particular case of Δr , the maximum ion diffusion correlation is obtained for its maximum value, $\Delta r^{(M)}$, which is above 70% (Fig. 6a). On the other hand, the smallest D_x correlation is found for the average interstitial residence time, which only amounts to $\approx 5\%$. As for the hopping frequency, the level of correlation with the ion diffusion coefficient is also positive but quite reduced ($\approx 20\%$). In most cases, the estimated correlations turn out to be statistically significant since the accompanying p -values are equal or smaller than 0.10 [6]. For a detailed description of the examined data, Fig. 6b shows the distribution of tracer ion diffusion coefficients calculated for each SSE family, which turn out to be quite diverse.

Based on this data-driven atomistic analysis, we may conclude that good superionic materials characterized by large ion diffusion coefficients should present large hopping lengths and hopping times but not necessarily high hopping frequencies and/or short interstitial residence

times (Fig. 6a). To put it differently, ample and timely, rather than short and too frequent, ionic hops appear to be associated with high ionic diffusion.

To gain further insight into the connections between high ionic diffusion and key atomistic descriptors, Supplementary Fig.3 shows the T -dependence of ν and Δr as evaluated for different SSE families. In general, it is found that the hopping frequency does not appreciably change with temperature whereas the average hopping distance noticeably increases upon increasing temperature. These results imply that the general T -induced ionic diffusion enhancement observed in SSE mostly is mediated by a surge in Δr rather than in ν . In turn, these findings appear to be coherent with the main conclusion presented in the preceding paragraph, namely, that the influence of the average hopping distance on fast-ion conduction exceeds that of the hopping frequency.

DISCUSSION

In the dilute-solution limit, the interactions between mobile ions are regarded as negligible hence the full ionic diffusion coefficient reduces to the tracer diffusion coefficient [19–21] (Methods) and its dependence on temperature can be expressed as [8, 18]:

$$D_x(T) = D_{x,0} \cdot \exp\left(-\frac{E_a}{k_B T}\right) \\ D_{x,0} \propto a^2 \nu_0, \quad (2)$$

where a is a hopping distance, E_a the activation energy barrier for ionic migration and ν_0 the hopping frequency.

The many mobile ion correlation results presented in previous sections show that the dilute-solution limit in

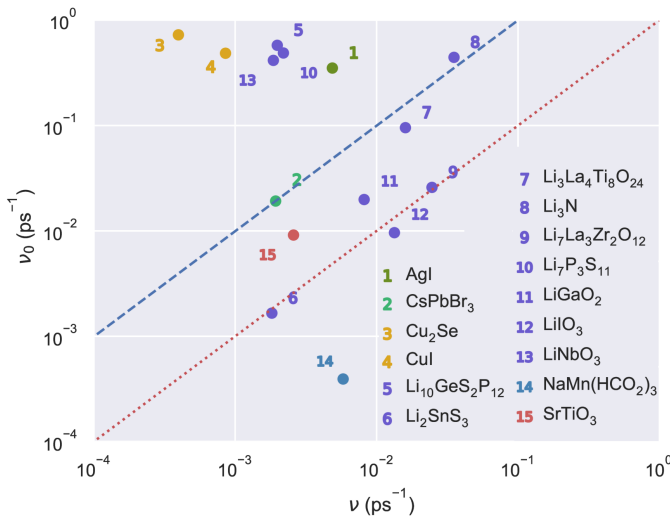


FIG. 7. Comparison of the hopping frequencies estimated for representative SSE in the dilute-solution limit, ν_0 , and by explicitly considering many-ion correlations, ν . The straight lines in the plot indicate the coincidence region in which the orders of magnitude of the two represented hopping frequencies coincide or differ to within a factor of 10 while fulfilling the condition $\nu \leq \nu_0$ (main text).

general does not apply to technologically relevant SSE, hence one may question the validity of Eq.(2) and other commonly employed formulas, like the Nerst-Einstein relation [Eq.(1) above], obtained under similar approximations. Aimed at quantitatively exploring this objection, we computed the hopping frequencies of all the SSE analysed in this study by using Eq.(2), ν_0 , which assumes the interactions between mobile ions to be negligible, and compared them with the values obtained directly from AIMD simulations with the IonDiff software [26], ν , which fully takes into consideration many-ion correlations. Since an undetermined proportionality factor enters Eq.(2), we constrain our comparative analysis to the orders of magnitude of the examined hopping frequencies.

Figure 7 shows our ν_0 and ν results obtained for 15 representative superionic materials. Due to the fact that the proportionality factor entering Eq.(2) may be of the order of 10^0 – 10^1 , we regard as coincident a pair of ν_0 – ν hopping frequencies differing within such a quantity and fulfilling the condition $\nu \leq \nu_0$ (i.e., the coincidence region delimited by the straight lines $\nu_0 = \nu$ –red– and $\nu_0 = 10\nu$ –blue– in Fig. 7). It is appreciated that by neglecting many-ion correlations the hopping frequency is slightly overestimated in average. In particular, 6 out of the 15 analysed materials are represented by points that clearly lie on the outer region above the selected coincidence interval. For instance, a large frequency discrepancy amounting from one to two orders of magnitude are obtained for $\text{Li}_{10}\text{GeS}_2\text{P}_{12}$, LiNbO_3 , Cu_2Se , CuI and AgI . On the other hand, the ν 's estimated for $\text{Li}_7\text{La}_3\text{Zr}_2\text{O}_{12}$, Li_2SnS_3 , SrTiO_3 and CsPbBr_3 , among others, agree fairly well with the approximate hopping

frequencies obtained from the corresponding tracer diffusion coefficients.

For Li-, Cu- and Ag-based SSE, the results enclosed in Fig. 7 indicate that ν_0 in general is a not a good approximation for ν since the former overestimates the latter. Contrarily, the points obtained for halide-, Na- and O-based SSE, as well as for some Li-based, are located inside or very close to the selected coincidence region meaning that ν_0 is a reasonably good approximation for ν . Based on these findings, along with those presented in previous sections (Fig. 4a), we can state that the hopping frequency of materials in which the correlations between mobile particles extend to many ions (only few ions) are likely to be poorly (fairly well) approximated by the tracer diffusion coefficient. This conclusion is quantitatively novel since failure of the relations obtained in the dilute-solution limit now can be directly associated with the average number of correlated mobile ions.

Finally, in order to quantify the influence of neglecting many-ion correlation on the calculation of the activation energy barrier for ionic migration, E_a , we estimated this quantity for $\text{Li}_7\text{La}_3\text{Zr}_2\text{O}_{12}$ (LLZO) and $\text{Li}_{10}\text{GeS}_2\text{P}_{12}$ (LGSP) considering both the tracer and full ionic diffusion coefficients (Methods) [19–21]. We selected these two materials because the first lies inside the coincidence interval defined for the ion hopping frequency while the second outside. For LLZO, it was found that when disregarding many-ion correlations E_a amounted to 0.16 eV whereas it decreased to 0.14 eV when accounting for them. For LGSP, we obtained similar results, in particular, 0.21 and 0.20 eV from the tracer and full ionic diffusion coefficients, respectively. Therefore, it may be concluded that the influence of neglecting many-ion correlations on the estimation of E_a appears to be less significant than for ν .

In conclusion, we have carried out a comprehensive and unsupervised many mobile ion correlation analysis for several families of SSE based on the k-means clustering approach, which has been implemented in the freely available open-source python code IonDiff [26]. An exponential decaying law is found to correctly describe the general probability density distribution governing the degree of concertation between many mobile ions in SSE. Accordingly, n -ion coordinated diffusion processes with $2 < n$ are found to be more frequent than pairwise coordinated diffusive events, although the latter hold the largest individual probability. For the particular case of Li-based SSE, the average number of correlated mobile ions is estimated to be 10 ± 5 and, interestingly, this result turns out to be practically independent of temperature. Furthermore, our data-driven analysis concludes that promising superionic materials characterized by large ion diffusion coefficients strongly and positively correlate with ample hopping lengths and long hopping times but not with high hopping frequencies and short interstitial residence times. Finally, it is shown that neglecting many-ion correlations generally leads

to a modest overestimation of the hopping frequency that roughly is proportional to the average number of correlated mobile ions. Overall, our work leverages the fundamental understanding of ionic transport and superionic materials and elaborates on the limitations of using formulas obtained in the dilute-solution approximation for describing technologically relevant SSE.

METHODS

First-principles calculations outline. *Ab initio* calculations based on density functional theory (DFT) [29] were performed to analyse the physico-chemical properties of bulk SSE. We performed these calculations with the VASP code [30] by following the generalized gradient approximation to the exchange-correlation energy due to Perdew *et al.* [31]. (For some halide compounds, likely dispersion interactions were captured with the D3 correction scheme developed by Grimme and co-workers [32].) The projector augmented-wave method was used to represent the ionic cores [33] and for each element the maximum possible number of valence electronic states was considered. Wave functions were represented in a plane-wave basis typically truncated at 750 eV. By using these parameters and dense \mathbf{k} -point grids for Brillouin zone integration, the resulting zero-temperature energies were converged to within 1 meV per formula unit. In the geometry relaxations, a tolerance of $0.005 \text{ eV}\cdot\text{\AA}^{-1}$ was imposed in the atomic forces.

First-principles molecular dynamics simulations. *Ab initio* molecular dynamics (AIMD) simulations based on DFT were performed in the canonical (N, V, T) ensemble (i.e., constant number of particles, volume and temperature) for all the analysed materials. The selected volumes were those determined at zero temperature hence thermal expansion effects were neglected; nevertheless, based on previously reported molecular dynamics tests [8], thermal expansion effects are not expected to affect significantly the estimation of ion-transport features at moderate temperatures. The concentration of ion vacancies in the non-stoichiometric compounds was also considered independent of the temperature and equal to $\sim 1\text{--}2\%$. The temperature in the AIMD simulations was kept fluctuating around a set-point value by using Nose-Hoover thermostats. Large simulation boxes containing $N \sim 200\text{--}300$ atoms were employed in all the cases and periodic boundary conditions were applied along the three supercell vector directions. Newton’s equations of motion were integrated by using the customary Verlet’s algorithm and a time-step length of $\delta t = 1.5 \cdot 10^{-3}$ ps. Γ -point sampling for integration within the first Brillouin zone was employed in all the AIMD simulations.

Our finite-temperature simulations typically comprised long simulation times of $t_{total} \sim 100$ ps. For

each material we typically ran an average of 3 AIMD simulations at different temperatures within the range $300 \leq T \leq 1200$ K, considering both stoichiometric and non-stoichiometric compositions [25]. Previous tests performed on the numerical bias stemming from the finite size of the simulation cell and duration of the molecular dynamics runs reported in work [8] indicate that the adopted N and t_{total} values should provide reasonably well converged results for the ion diffusivity and vibrational density of states of SSE.

The mean squared displacement (MSD) was estimated with the formula:

$$\text{MSD}(t) = \frac{1}{N(N_t - n_t)} \cdot \sum_{i,j=1}^{N, N_t - n_t} |\mathbf{r}_i(t_j + t) - \mathbf{r}_i(t_j)|^2, \quad (3)$$

where $\mathbf{r}_i(t_j)$ represents the position of the mobile ion i at time $t_j (= j \cdot \delta t)$, t a lag time, $n_t = t/\delta t$, N the total number of mobile ions, and N_t the total number of time steps (equivalent to ~ 100 ps). The maximum n_t was chosen equal to $N_t/2$ (equivalent to ~ 50 ps) in order to accumulate enough statistics to reduce significantly the $\text{MSD}(t)$ fluctuations at large t ’s. The tracer diffusion coefficient, D , then was obtained based on the Einstein relation:

$$D = \lim_{t \rightarrow \infty} \frac{\text{MSD}(t)}{6t}. \quad (4)$$

In practice, we considered $0 < t \leq 50$ ps and estimated D by performing linear fits to the averaged $\text{MSD}(t)$ obtained over the last 25 ps. When taking into account many-ion correlations, the full diffusion coefficient was estimated by considering additional i - j particle positions crossed terms in Eq.(3) [21].

Spatio-temporal correlation function. The van Hove correlation function, $G(\Delta r, \Delta t)$, provides information on the spatio-temporal distribution of particles during a simulation. This two-dimensional function can be intuitively divided into a “self”, G_s , and a “distinct”, G_d , part. The former describes the displacements of a specific particle throughout time while the latter describes the relations of a particle with the rest, namely:

$$\begin{aligned} G(r, t) &= \frac{1}{N} \left\langle \sum_{i,j=1}^N \delta(r - |\mathbf{r}_i(t_0 + t) - \mathbf{r}_j(t_0)|) \right\rangle \quad (5) \\ &= G_s(r, t) + G_d(r, t) \end{aligned}$$

where \mathbf{r} represent the atomic positions, indices i and j run over all the mobile particles, $\delta(x)$ is the Dirac delta function, t_0 and arbitrary time, and averages are estimated over the total simulation time. The “self” and “distinct” parts of the van Hove correlation function are then defined like:

$$\begin{aligned} G_s(r, t) &= \frac{1}{N} \left\langle \sum_{i=1}^N \delta(r - |\mathbf{r}_i(t_0 + t) - \mathbf{r}_i(t_0)|) \right\rangle \quad (6) \\ G_d(r, t) &= G(r, t) - G_s(r, t). \end{aligned}$$

IonDiff software. The freely available open-source python code `IonDiff` [26] is based on an unsupervised k-means clustering algorithm (see next section for additional details). `IonDiff` assigns a spatial point (i.e., centre of vibration) to every particle in the simulation supercell at each simulated time step. The centers of vibration then are compared with the stoichiometric equilibrium lattice so that (1) ion-hopping events can be straightforwardly identified without the need of defining any arbitrary length or parameter, and (2) metastable positions can be also readily determined. The residence time for a particular metastable position is estimated like the number of simulation steps associated with that location averaged over all the particles. The only required input files are two: (1) one containing the positions of the particles throughout the whole simulation (e.g., XDATCAR file in the case of VASP calculations), and (2) another detailing the length and number of time steps (e.g., INCAR file in the case of VASP calculations).

K-means clustering. The unsupervised algorithm devoted to identifying diffusive particles and their respective paths in molecular dynamics simulations is based on the k-means clustering approach. The implementation of the k-means clustering algorithm in the Scikit-learn python package [35] was used in practice. The number of clusters at each time step, K , was selected based on the average silhouette method. In particular, the chosen K corresponds to that which maximises its average

value over all possible $2 \leq K$ cases (see main text). An arbitrary but reasonable confidence threshold value of 0.7 was imposed for the silhouette coefficients, S (Eq.7). This means that if the maximum average silhouette coefficient amounted to less than 0.7, the condition $K = 1$ was automatically imposed.

Being M_I the number of points in cluster I , with $M_I > 1$, the silhouette coefficient for a data point in that cluster, i , is mathematically defined like:

$$S(i) = \frac{b(i) - a(i)}{\max[a(i), b(i)]}, \quad (7)$$

where

$$a(i) = \frac{1}{M_I - 1} \sum_{j=1, j \neq i}^{M_I} \|\mathbf{r}_j - \mathbf{r}_i\|^2 \quad (8)$$

$$b(i) = \min_{J \neq I} \frac{1}{M_J} \sum_{j=1}^{M_J} \|\mathbf{r}_j - \mathbf{r}_i\|^2. \quad (9)$$

By proceeding in this manner, the similarity of a point within its own cluster and its dissimilarity with the others were simultaneously optimized.

DATA AVAILABILITY

The data that support the findings of this study are available from the corresponding authors upon reasonable request.

-
- [1] Famprakis, T., Canepa, P., Dawson, J. A., Islam, M. S. and Masquelier, C. Fundamentals of inorganic solid-state electrolytes for batteries. *Nat. Mater.* **18**, 1278 (2019).
- [2] Sapkota, P., Boyer, C., Dutta, R. *et al.* Planar polymer electrolyte membrane fuel cells: Powering portable devices from hydrogen. *Sustainable Energy Fuels* **4**, 439 (2020).
- [3] Mofarah, S. S., Adabifiroozjaei, E., Yao, Y. *et al.* Proton-assisted creation of controllable volumetric oxygen vacancies in ultrathin CeO_{2-x} for pseudocapacitive energy storage applications. *Nat. Commun.* **10**, 2594 (2019).
- [4] Aznar, A., Lloveras, P., Romanini, M. *et al.* Giant barocaloric effects over a wide temperature range in superionic conductor AgI. *Nat. Commun.* **8**, 1851 (2017).
- [5] Bachman, J. C., Muy, S., Grimaud, A., Chang, H.-H., Pour, N., Lux, S. F., Paschos, O., Maglia, F., Lupart, S., Lamp, P., Giordano, L. and Shao-Horn, Y. Inorganic solid-state electrolytes for lithium batteries: Mechanisms and properties governing ion conduction. *Chem. Rev.* **116**, 140 (2016).
- [6] López, C., Emperador, A., Saucedo, E., Rurali, R. and Cazorla, C. Universal ion-transport descriptors and classes of inorganic solid-state electrolytes. *Mater. Horiz.* **10**, 1757 (2023).
- [7] Muy, S., Schlem, R., Shao-Horn, Y. and Zeier, W. G. Phonon-ion interactions: Designing ion mobility based on lattice dynamics. *Adv. Energy Mater.* **11**, 2002787 (2021).
- [8] Sagotra, A., Chu, D. and Cazorla, C. Influence of lattice dynamics on lithium-ion conductivity: A first-principles study. *Phys. Rev. Mater.* **3**, 035405 (2019).
- [9] Muy, S., Bachman, J. C., Giordano, L., Chang, H.-H., Abernathy, D. L., Bansal, D., Delaire, O., Hori, S., Kanno, R., Maggia, F., Lupart, S., Lamp, P. and Shao-Horn, Y. Tuning mobility and stability of lithium ion conductors based on lattice dynamics. *Energy Environ. Sci.* **11**, 850 (2018).
- [10] Zhang, Z., Nazar, L.F. Exploiting the paddle-wheel mechanism for the design of fast ion conductors. *Nat. Rev. Mater.* **7**, 389 (2022).
- [11] Gupta, M. K., Ding, J., Osti, N. C., Abernathy, D. L., Arnold, W., Wang, H., Hood, Z. and Delaire, O. Fast Na diffusion and anharmonic phonon dynamics in superionic Na_3PS_4 . *Energy Environ. Sci.* **14**, 6554 (2021).
- [12] Ding, J., Niedziela, J., L., Bansal, D., Wang, J., He, X., May, A. F., Ehlers, G., Abernathy, D. L., Said, A., Alatas, A., Ren, Y., Arya, G. and Delaire, O. Anharmonic lattice dynamics and superionic transition in AgCrSe_2 . *Proc. Natl. Acad. Sci.* **117**, 3930 (2020).

- [13] Ren, Q., Gupta, M. K., Jin, M., Ding, J., Wu, J., Chen, Z., Lin, S., Fabelo, O., Rodríguez-Velamazán, J. A., Kofu, M., Nakajima, K., Wolf, M., Zhu, F., Wang, J., Cheng, Z., Wang, G., Tong, X., Pei, Y., Delaire, O. and Ma, J. Extreme phonon anharmonicity underpins superionic diffusion and ultralow thermal conductivity in argyrodite Ag_8SnSe_6 . *Nat. Mater.* **22**, 999 (2023).
- [14] Xu, Z., Chen, X., Zhu, H. and Li, X. Anharmonic cation-anion coupling dynamics assisted lithium-ion diffusion in sulfide solid electrolytes. *Adv. Mater.* **34**, 2207411 (2022).
- [15] Zhang, Z., Zou, Z., Kaup, K., Xiao, R., Shi, S., Avdeev, M., Hu, Y.-S., Wang, D., He, B., Li, H., Huang, X., Nazar, L. F., Chen, L. Correlated migration invokes higher Na^+ -ion conductivity in NaSICON-type solid electrolytes. *Adv. Energy Mater.* **9**, 1902373 (2019).
- [16] Jalem, R., Tateyama, Y., Takada, K., Nakayama, M. First-principles DFT study on inverse Ruddlesden-Popper tetragonal compounds as solid electrolytes for all-solid-state Li^+ -ion batteries. *Chem. Mater.* **33**, 5859 (2021).
- [17] He, X., Zhu, Y. and Mo, Y. Origin of fast ion diffusion in super-ionic conductors. *Nat. Commun.* **8**, 15893 (2017).
- [18] Ven, A. V., Ceder G., Asta, M. and Tapesch, P. D. First-principles theory of ionic diffusion with nondilute carriers. *Phys. Rev. B* **64**, 184307 (2001).
- [19] Molinari, N., Xie, Y., Leifer Y., Marcolongo, A., Kornbluth, M. and Kozinsky, B. Spectral denoising for accelerated analysis of correlated ionic transport. *Phys. Rev. Lett.* **127**, 025901 (2021).
- [20] Marcolongo, A. and Marzari, N. Ionic correlations and failure of Nernst-Einstein relation in solid-state electrolytes. *Phys. Rev. Mater.* **1**, 025402 (2017).
- [21] Sasaki, R., Gao, B., Hitosugi, T. and Tateyama, Y. Nonequilibrium molecular dynamics for accelerated computation of ion-ion correlated conductivity beyond Nernst-Einstein limitation. *npj Comput. Mater.* **9**, 48 (2023).
- [22] France-Lanord, A. and Grossman, J. C. Correlations from ion pairing and the Nernst-Einstein equation. *Phys. Rev. Lett.* **122**, 136001 (2019).
- [23] Murugan, R., Thangadurai, V. and Weppner, W. Fast lithium ion conduction in garnet-type $\text{Li}_7\text{La}_3\text{Zr}_2\text{O}_{12}$. *Angew. Chem. Int. Ed.* **46**, 7778 (2007).
- [24] Islam, S. M. K. N., Mayank, P., Ouyang, Y., Chen, J., Sagotra, A. K., Li, M., Cortie, M. B., Mole, R., Cazorla, C., Yu, D., Wang, X., Robinson, R. A. and Cortie, D. L. Copper diffusion rates and hopping pathways in superionic Cu_2Se . *Acta Mater.* **215**, 117026 (2021).
- [25] The DFT-AIMD database analyzed in this work can be found at the URL: <https://superionic.upc.edu/>
- [26] López, C., Rurali, R. and Cazorla, C. <https://github.com/IonRepo/IonDiff>
- [27] He, X., Bai, Q., Liu, Y., Nolan, A. M., Ling, C. and Mo, Y. Crystal structural framework of lithium super-ionic conductors. *Adv. Ener. Mater.* **9**, 1902078 (2019).
- [28] Winter, G. and Gómez-Bombarelli, Simulations with machine learning potentials identify the ion conduction mechanism mediating non-Arrhenius behavior in LGPS. *J. Phys. Energy* **5**, 024004 (2023).
- [29] Cazorla, C. and Boronat, J. Simulation and understanding of atomic and molecular quantum crystals. *Rev. Mod. Phys.* **89**, 035003 (2017).
- [30] Kresse, G. and Furthmüller, J. Efficient iterative schemes for *ab initio* total-energy calculations using a plane-wave basis set. *Phys. Rev. B* **54**, 11169 (1996).
- [31] Perdew, J. P., Burke, K. and Ernzerhof, M. Generalized gradient approximation made simple. *Phys. Rev. Lett.* **77**, 3865 (1996).
- [32] Grimme, S., Antony, J., Ehrlich, S. and Krieg, S. A consistent and accurate *ab initio* parametrization of density functional dispersion correction (DFT-D) for the 94 elements H-Pu. *J. Chem. Phys.* **132**, 154104 (2010).
- [33] Blöchl, P. E. Projector augmented-wave method. *Phys. Rev. B* **50**, 17953 (1994).
- [34] Togo, A. and Tanaka, I. First principles phonon calculations in materials science. *Scr. Mater.* **108**, 1 (2015).
- [35] Pedregosa, F., Varoquaux, G, Gramfort, A. *et al.* Scikit-learn: Machine Learning in Python. *J. Mach. Learn. Res.* **12**, 2825 (2011).

ACKNOWLEDGEMENTS

C.C. acknowledges support from the Spanish Ministry of Science, Innovation and Universities under the fellowship RYC2018-024947-I, PID2020-112975GB-I00 and grant TED2021-130265B-C22. The authors thankfully acknowledge the CSIC under the “JAE Intro SOMdM 2021” grant program and the computer resources at MareNostrum and the technical support provided by Barcelona Supercomputing Center (FI-1-0006, FI-2022-2-0003, FI-2023-1-0002, FI-2023-2-0004 and FI-2023-3-0004). R.R. acknowledges financial support from the MCIN/AEI/10.13039/501100011033 under Grant No. PID2020-119777GB-I00, the Severo Ochoa Centres of Excellence Program (CEX2019-000917-S) and the Generalitat de Catalunya under Grant No.2017SGR1506.

AUTHOR CONTRIBUTIONS

C.C. conceived the study and planned the research. C.L. developed the analysis algorithms and applied them on a DFT-AIMD database previously generated by C.C., R.R. and C.L. Results were discussed by all the authors. The manuscript was written by C.L. and C.C. with substantial input from the rest of authors.

COMPETING INTERESTS

The authors declare no competing interests.